Turbulent convective heat transfer of silica oxide nanofluid through corrugated channels: An experimental and numerical study

Raheem K. Ajeel [a,b,*], W.S.-I. Salim [a], K. Sopian [c], M.Z. Yusoff [d], Khalid Hasnan [a], Adnan Ibrahim [c], Ali H.A. Al-Waeli [c]

[a] Faculty of Mechanical and Manufacturing Engineering, Universiti Tun Hussein Onn Malaysia, 86400 Parit Raja, Batu Pahat, Johor, Malaysia
[b] Department of Mechanical Engineering, College of Engineering, University of Babylon, Babylon, Iraq
[c] Solar Energy Reasearch Institute, Universiti Kebargsaan Malaysia, 43600 Bangi, Selangor, Malaysia
[d] Centre for Advanced Computational Engineering, Universiti Tenaga Nasional, Selangor 43000, Malaysia

ARTICLE INFO

ABSTRACT

Combining a corrugated surface and nanofluids technologies have caused attracted significant interest to develop the ability of compact heat exchangers in order to produce more efficient and reliable thermal systems. In this paper, the forced convective turbulent flow of SiO_2-water nanofluid through different corrugated channels is studied numerically and experimentally. All studies are performed for the straight channel (SC) and different two corrugated channels, namely semicircle corrugated channel (SCC) and trapezoidal corrugated channel (TCC) over Reynolds number ranges of 10000–30000. SiO_2 nanoparticles suspended in distilled water with two particle volume fractions (1% and 2%) were successfully prepared and tested. Numerically, the discussion and analysis on heat transfer and flow characteristics which including velocity, isotherms contours, turbulence kinetic energy, vortices magnitude are provided. The results show that the corrugation profile has a significant impact on heat transfer enhancement compared to the straight profile. Also, silica nanofluid shows a better heat transfer in comparison with the base fluid. The new style of trapezoidal corrugated channel offers the best heat transfer enhancement. This indicated that this geometry with silica nanofluid can improve the heat transfer significantly with a reasonable increase in pressure drop. The results for the numerical outcomes and experimental data are in good agreement.

© 2019 Elsevier Ltd. All rights reserved.

1. Introduction

Although there are different industrial applications and uses for heat exchangers, the efforts of researchers have been to increase efficiency and reduce weight and size. In this light, corrugated surfaces have emerged as one of the best passive ways to increase efficiency and improve heat transfer despite increased pressure. Corrugated walls depend on manipulating the fluid direction of the main flow, which helps induce secondary flow vortexes that enhance heat transfer. This passive method greatly influences heat transfer enhancement. The use of traditional fluids in this technique has been limited due to their somewhat lackluster thermal properties. Therefore, the prime obstacle to improving heat transfer processes is the poor thermophysical properties of these liquids. The introduction of nanoparticles into conventional liquids offers a viable solution to improving the thermal properties of

these liquids. Experimental and numerical studies have shown that the ability and potential of the resulting mixture, called a nanofluid, promotes heat transfer. In spite of using nanofluids to boost the thermal performance of the compact heat transfer, clogging in the process may be found in the tested channel when the fluid with large particles were employed and due to the effect of long-term instability.

Many studies in different regimes were conducted on heat transfer characteristics that used traditional fluids in different configurations of corrugated channels [1–9]. Investigators have revealed that heat transfer in such channels has been improved though and increased pressure drop penalty.

Many studies have numerically and experimentally examined nanofluids to determine their flow and thermal characteristics through straight channels. Numerically, by employing single and two-phase models of nanofluid, Fard et al. [10] studied the laminar convective heat transfer of nanofluids in a circular tube under constant wall temperature condition using the CFD approach. The results showed that heat transfer coefficient (HTC) dramatically

Nomenclature

A	area, mm^2		T	temperature, K
Cp	specific heat capacity (J/kg K)		TCC	trapezoidal-corrugated channel
C$_f$	skin friction coefficient			
ER	enhancement ratio		*Greek symbols*	
D$_h$	hydraulic diameter, mm		μ	dynamic viscosity of the fluid (kg/m s)
d$_p$	nanoparticle diameter, nm		ρ	density (kg/m^3)
HTC	heat transfer coefficient (W/m^2 K)		ε	turbulent kinetic dissipation (m^2/s^2)
k	thermal conductivity (W/m K)		τ	wall shear stress (Pa)
$\dot{m}$	mass flow rate, kg/s		σ_k	diffusion Prandtl number for k
Nu	Nusselt number		ϕ	nanoparticle volume fraction
PEC	thermal-hydraulic performance			
PR	pressure ratio, ($\Delta p_{corr}/\Delta p_{SC)}$		*Subscripts*	
Δp	pressure drop (Pa)		corr	corrugated channel
Pr	Prandtl number, $Pr = \frac{cp\mu}{k}$		f	fluid
Q$_f$	heat received by fluid, w		in	inlet
q	heat flux (W/m^2)		av	average
Re	Reynolds number, $Re = \frac{\rho u_i D_h}{\mu}$		out	outlet
SiO$_2$	silicon dioxide		nf	nanofluid
SCC	semicircle-corrugated channel		p	particles
SC	straight channel		w	wall
SS	shear stress (Pa)			

increased with increasing volume fraction of nanoparticles (ϕ). Abdolbaqi et al. [11] performed a numerical study to analyze the heat transfer enhancement of nanofluids with different volume concentrations under turbulent flow through a straight channel with a constant heat flux condition. The study was conducted for Reynolds number range of 10000–100000, different nanoparticles of TiO$_2$ and CuO, and different volume concentrations of 1–3%. The results illustrated that the enhancement of Nusselt number and wall shear stress increase with increasing volume fractions. Also, nanofluids were considered to have great potential for heat transfer enhancement.

Rostamani et al. [12] numerically analyzed the turbulent flow of nanofluids with different volume concentrations of nanoparticles flowing through a two-dimensional duct under constant heat flux condition. The study employed different nanofluids of Al$_2$O$_3$, CuO, and TiO$_2$ suspended in water as working fluids over Reynolds number range of 20,000–100,000. The results revealed that, of the three employed nanofluids, the CuO had the best heat transfer. It was also found that by increasing the volume concentration, the wall shear stress and heat transfer rates increase.

Sajadi and Kazemi [13] revealed that the heat transfer coefficient (HTC) of nanofluid (titanium dioxide/water) increases with the addition a small amount of nanoparticles. Also, they presented some correlations for Nusselt number as a function of titanium dioxide nanoparticles based on experimental data.

Heris et al. [14] told that Al$_2$O$_3$/water nanofluid has significantly higher heat transfer coefficients compared with the results for the pure water.

Few investigations have been performed that dealt with the heat transfer and flow characteristics of nanofluid using corrugated channels. For instance, numerically, by employing a sinusoidal wavy channel, Esmaeili et al. [15] showed that the heat transfer enhancement ratio (ER) and shear stress (SS) increase with using nanofluid. Furthermore, it was found that Nusselt number increases with increases of Reynolds number.

Ajeel et al. [16–21] performed a series of numerical investigations on corrugated channels using different types of nanofluids. They showed that the average Nusselt number (Nu_{av}) was dramatically enhanced compared to the smooth channels due to the corrugation profile effects, and remarkable pressure drop was

obtained as well. In another works, they also [22–24] investigated the impact of geometrical parameters on PEC in various corrugated channels. The simulation results clarified that the ratio of height-to-width was more effective than the pitch-to-length ratio in terms of PEC. Also, it is shown that by increasing ϕ and *Re*, the flow structures changes.

Experimentally, using horizontal helically corrugated tube and TiO$_2$ nanofluids, Naphon and Wiriyasart [25] told that the thermal properties of nanofluid greatly impacted the thermal performance and heat transfer. Pavlovic et al. [26] experimentally examined the use of various nanofluids as working fluids in a solar dish collector with smooth and corrugated absorber tube where the volume concentrations of nanoparticles in the base fluid were up to 5%. Experiments conducted for different particles of Al$_2$O$_3$, Cu, CuO and TiO$_2$ dispersed on thermal oil and water. The results showed that a maximum exergetic efficiency of 12.29% was recorded for the Cu-oil nanofluid. Utilization of Cu nanoparticle was the most suitable exergetically among the examined cases.

Khoshvaght-Aliabadi et al. [27] experimentally studied on forced convective flows of different nanofluids through a corrugated wavy channel at a constant wall temperature condition for a concentrations range of 0.1–0.4%. Experiments carried out for different nanoparticles of SiO$_2$, TiO$_2$, ZnO, Fe$_2$O$_3$, Al$_2$O$_3$, Cu and CuO, and types of base fluid (deionized water–ethylene glycol mixture), for different volumetric flow rates. The major experimental result showed that the corrugated wavy channels heat transfer was better than smooth channel. Also, they detected that thermal performance improves with increasing ϕ.

Alfaryjat et al. [28] found numerically that the thermal performance for all nanofluids tested increases with increase of nanoparticles volume fraction and decrease of the size of particles. Fotukian and Nasr Esfahany [29] indicated that addition of small amounts of nanoparticles (γ-Al2O3) to the base fluid (water) augmented heat transfer remarkably. Numerically, using microchannel and Cu–water nanofluid, Raisi et al. [30] revealed that heat transfer was affected by both volume fraction and slip velocity. The experimental results of Khoshvaght-Aliabadi et al. [31] referred that the heat transfer rate was increased by using nanofluids and it was slightly affected by the type of nanofluids.

Manca et al. [32] numerically investigated on forced convection with nanofluids, composed by water and Al$_2$O$_3$ nanoparticles, in a two-dimensional channel for Reynolds number from 20,000 to 60000. The results showed that heat transfer enhancement increases with the particle volume concentration but it is accompanied by increasing required pumping power.

Ahmed et al. [33] showed numerically that the corrugations had significantly improved the thermal performance compared to the flat profile. Also, Nu_{av} number and the pressure drop for all tested channels increase with increasing the nanoparticles volume fraction and flow Reynolds number. The experimental results of Ali and Arshad [34] revealed that the heat transfer rate and the pressure drop for the nanofluid (TiO$_2$-water) are higher than the base fluid. Also, they showed that thermal performance was strongly dependent on heating power.

Numerically and experimentally, using trapezoidal, sinusoidal, and straight channels and a SiO2-water nanofluid, Ahmed et al. [35] showed that Nusselt number, pressure drop and heat transfer enhancement for all channels increase with increasing the nanoparticles volume fraction. Also, the heat transfer enhancement for the trapezoidal channel is higher than the other channels.

In spite of the enhancement heat transfer by nanofluids and corrugated channels having been previously studied and reported in the literature review as shown, an explanation for the influence of corrugation architecture together with different nanofluids and nanoparticle volume on heat transfer characteristics is still limited. This is the motivation for this study. Also, all previous experimental works that employed corrugated channels as test modules only focused on familiar forms. Therefore, the need to test new forms such as semicircle and trapezoidal channels is another motivation for this study. Thus, this study aims to investigate the experimentally turbulent forced convective flow of a silicon dioxide-water nanofluid with two volume fractions in two types of corrugated channels, namely a Trapezoidal Corrugated Channel (TCC) and Semicircle Corrugated Channel (SCC) in addition to the straight channel (SC). In addition to the experiment, numerical simulations are conducted to show the flow structure of the nanofluids through the consideration channels. Finally, the experiments are conducted under constant heat flux conditions over Re ranges of 10,000–30000.

2. Preparation of nanofluids

In this work, nanoparticles of SiO2 with average diameter of 20 nm (Purchased from Novascientific Resources (M) Sdn. Bhd.)

Fig. 1. FESEM photograph of silica dioxide nanoparticles.

were used to prepare the nanofluid. Before preparing the nanofluid and for purpose of collecting the chemical characteristics and elemental analysis, several tests have been done. For instance, to check particle size, shape, and agglomeration visualization, Field Emission Scanning Electron Microscopy (FESEM) is employed. An FESEM is a microscope that utilizes electrons (particles with a negative charge) instead of light. The (FESEM) image allowed us to determine the size of the nanoparticles prior to it being dispersed in base fluid. The findings of this test show that SiO$_2$ has approximately spherical form with size around 20 nm as shown in Fig. 1. Two other tests, including an Electron Dispersion X-ray (EDX) image and an Electron Dispersion Spectroscopy (EDS), are conducted as shown in Figs. 2 and 3, respectively. EDX and EDS are helpful techniques to give a better understanding of chemical analysis such as morphological composition. This equipment is attached to the FESEM to facilitate the collection of elemental information from the sample under examination. According to above characterization techniques, it is observed that the nanoparticles are well dispersed with certain level of agglomeration.

Because the two-step technique is widely used and it is also cheaper than the one-step technique, it was employed to prepare silica nanofluids in this study. In addition, two-step techniques are more effective than one-step techniques in producing a nanofluid solution efficiently at large scale. In general, dry powders (nanopowder) are formed using physical and chemical methods in the first step of preparation (done by supplier). This was followed by the second step, which involved dissolving the powder from the first step in the base fluid with the help of a mechanical or magnetic stirrer and ultrasonic shaker to obtain a homogeneous solution.
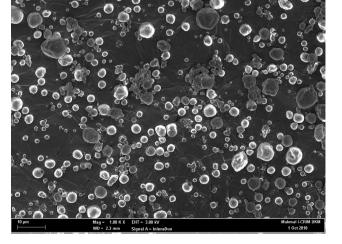
In this study, nanofluids with SiO$_2$ nanoparticles desired volume fractions of 1.0% and 2.0% are prepared by dispersing specific amounts of nanoparticles into distilled water. Then the nanoparticle mixture in distilled water is transferred to an ultrasonic shaker bath with a volume of 12 L (TELSONIC ULTRASONICS CT-12) to obtain homogeneous suspensions and break up any potential nanoparticles clusters. The perfect setting for the ultrasonic bath was 800 W and 30 kHz with a maximum time of 90 min. During all experiments, the nanofluid solution was stable and uniform and no sedimentation was observed. To avoid influencing thermophysical properties, no surfactant was used as stabilizer or dispersive in the preparation of nanofluid [35].

The agglomeration of nanoparticles results in not only the settlement and clogging of channels but also the decreasing of thermal conductivity of nanofluids. Therefore, the investigation on stability is also a key issue that influences the properties of nanofluids for application, and it is essential to ensure that the nanofluid mixture stays homogeneous and stable during the experiments period. Herein, the stability and uniformity of nanofluid was measured by two methods. Firstly, the mixture has been placed under observation (visual test) for 150 h by using open containers. After this period, a few small clusters of nanoparticles were observed for nanofluids at 2% volume fractions. By this way, this can be considered as confirming that the mixture is stable fluid. Secondly, by measuring the viscosity of mixture over 24 h at a constant temperature of 25 °C. The outcomes showed that the viscosity is constant during the test which is indicating the stability of the mixture over that period as illustrated in Fig. 4.

The amount of SiO$_2$ nanopowder required for nanofluid preparation is given by the following equation [36]:

$$\phi = \frac{\frac{m_p}{\rho_p}}{\frac{m_p}{\rho_p} + \frac{m_f}{\rho_f}} \tag{1}$$

Rearranging the Eq. (1) provides the following:

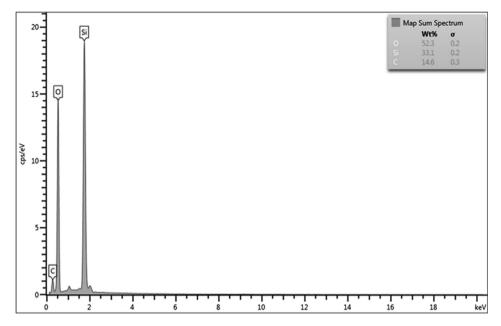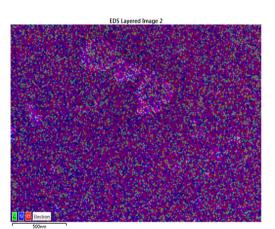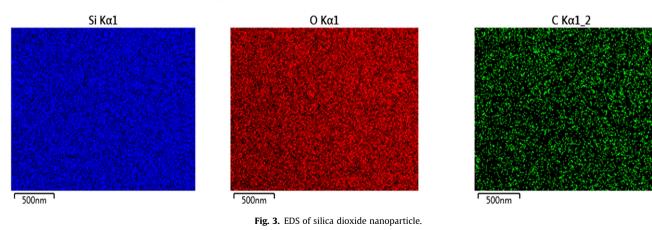**Fig. 2.** EDX of silica dioxide nanoparticles.

Fig. 3. EDS of silica dioxide nanoparticle.

$$m_p = \rho_p \left[\frac{\phi}{1-\phi} \right] \left[\frac{m_f}{\rho_f} \right] \qquad (2)$$

It should be noted that the amount of SiO$_2$ (m_p) added to 100 ml of distilled water (m_f) had a density (ρ_p) of 2220 kg/m^3.

3. Thermophysical properties of nanofluids

In this study, silica nanofluid thermophysical properties of density, viscosity, thermal conductivity, and specific heat were experimentally determined. The transient hot-wire method was used to
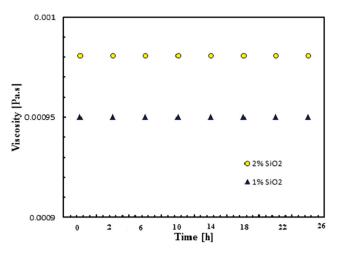
Fig. 4. Viscosity of SiO₂-water nanofluids at 25 °C over 24 h.

measure thermal conductivity using a thermal property analyzer KD2 Pro system (Decagon Devices). A Brookfield DV3T-7INCH Rheometer was used to measure viscosity while a density meter (DH-300L, Kyoto Electronics) was employed to measure density. Finally, a differential scanning calorimeter (PerkinElmer model DSC 4000) was utilized to determine nanofluid specific heat. All density, viscosity, specific heat, and thermal conductivity experiments were repeated three times to confirm repeatability, and the mean value was taken to reduce the uncertainty resulting from the random error in the measurement. Also, it should be noted that the thermophysical property measurement process was performed in an ideal laboratory environment that was available in the Solar Energy Research Institute (SERI), National University of Malaysia. Properties of the water and nanofluids are shown in Table 1.

4. Experimental setup

4.1. Apparatus and procedure

The experimental facility for this study is presented in Fig. 5. The test loop mainly consisted of: (1) cooling unit, (2) test section, (3) a set of thermocouples, (4) flow meter, (5) plate heater, (6) data logger, (7) differential pressure transducer, (8) pump, (9) power regulator and multimeter, and (10) working fluid tank.

A pump (0.7 HP) is employed to push the operating fluid from the reservoir to flow through the test loop. To achieve boundary conditions for the parallel corrugated walls of the test section, two electrical heater plates are employed to heat the parallel walls. The heater plates fixed to the rear faces of these walls have a maximum power of 320 W for each heater. Fiber-glass insulation (2 layers 50 mm thick) surrounded the test module to reduce heat loss from the test section to the environment. The electric circuit also contained the AC power regulator (W5SP4vo30-24J, SPINE, with ±0.1 accuracy) and digital multimeter (BK PRECISION, 2831C, with ±1% FS accuracy). By controlling the voltage and current through the power regulator and taking measurements through the digital multimeter, the required heat flux was provided. Six calibrated (k-type) temperature thermocouples with

0.1 °C accuracy are fixed at the rear face of the upper wall of channel to measure the temperature distribution along the wall of the test section. These thermocouples are inserted through the holes, which are drilled with 2 mm diameter from the back side of the channel walls, and fixed using thermal epoxy. The holes are located 30, 60, 90, 120, 150, and 180 mm from the inlet of the test section. It should be noted that six holes are drilled in the heater in order to pass the wires of thermocouples that are used to measure the heated wall temperature of the test section. The inlet and outlet temperatures of fluid flow are measured by two temperature probes (RTD with an accuracy of 0.1 °C) which are inserted into the flow directly. All thermocouples used in this study were calibrated by using ice path.

Differential pressure transducers (DPG409-001DWU Omega, USA, ±0.075% accuracy) are also mounted across the test section to measure pressure drop. By passing through the chiller unit (SPH20N-18-4227, refrigerant R22, Compressor 1 kW), the working fluid loses the heat it has gained from the test section to maintain a constant temperature at entry (27). The inlet bulk temperature is controlled by using the control board of chiller. To collect data (thermocouples and pressure transducer) and convert data into PC, a data logger system is used with a DAQ manager program. The data logger type MultiCon SIMEX (16 channels) made in Germany is used in this study.

Furthermore, to measure the flow rate of the fluid, a digital flow meter (Ada-K24F1-1, HaiHuiLai, ±5% accuracy) is placed between the pump and inlet of the upstream section. A bypass line with a valve is used to adjust the flow rate of the pump.

Initial experiments on heat transfer and pressure drop are conducted with base fluid which is water as a working fluid. Later nanofluids with different volume fractions are introduced into the system.

After the flow reached a steady state conditions and energy balance is obtained, and a constant temperature bath of 27 °C is achieved. Flow rate, pressure drop across the test module, test module thermocouples temperatures, and bulk water temperature at the inlet and the outlet of the test module are recorded. The test module is changed into a semicircle-corrugated channel and all the above steps are repeated.

4.2. Test section

Fig. 6 shows the 2-D and 3-D physical domain of the test modules assigned the corrugated channels in this study while Fig. 7 illustrates the front view of designed and fabricated module. It is composed of stainless steel corrugated walls (top and bottom) and straight walls (side walls). The corrugated walls are 50 mm wide, 200 mm long, and 8 mm thick. The corrugated wall height h was 2.5 mm with a longitudinal pitch (p = 1.5H). The width of corrugated wall (w) is 5 mm. Those walls are created using a precision sawing technique on a Bridgeport CNC machine. The smooth walls are fabricated from acrylic (8 mm thick) and assembled with the corrugated walls to contain the test module. After assembly, the width and height of the test module are 50 mm and 10 mm, respectively. To reduce heat loss, the smooth and corrugated walls are assembled and fixed using bolts and thermal epoxy. Table 2 details the geometrical structure of the corrugated channels used in the experiments.

Table 1
Thermophysical properties of water and SiO₂-water nanofluids with different volume fractions at 25 °C.

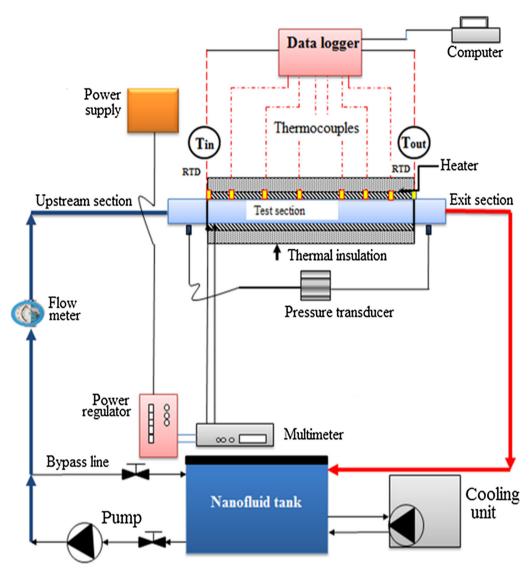| Fluid	ρ (kg/m³)	C_p (J/kg K)	K (W/m K)	μ (kg/m s)
Water	997.9	4144.0	0.6094	0.000943
Water + 1.0% SiO₂	1009.0	4141.2	0.615	0.00095
Water + 2.0% SiO₂	1021.1	4114.1	0.6289	0.000981

Fig. 5. Layout of the experimental setup.

4.3. Developing and exit sections

To create suitable conditions for the inlet and outlet flow of test module, two flat sections (developing and exit) located upstream and downstream the test section, respectively, were used. These sections are fabricated from 6 mm thick acrylic sheets. The developing section has an axial length of 800 mm while the length of the exit section is 100 mm. Each section have a cross sectional area of 10 mm height and a 50 mm width, which is identical to the inlet and outlet of test module. Two flanges, which are fabricated from 10 mm thick acrylic sheet, are attached to both section ends in addition to the test module using screws and thermal epoxy. However, the test module is directly connected to the entry and exit using flanges with bolts. Therefore, the replace process for the test module is very easy, with three modules being tested and reconnected. All test module entry and exit sections were fabricated by PRIME TECH SERVICES SDN BHD, Malaysia.

4.4. Data reduction

The experimental data recorded in this study, such as bulk fluid temperature, wall temperature, pressure drop, volume flow rate, voltage, and current are employed to estimate the Nusselt number and pressure drop. The heat supplied to the electrical heaters is given as [35]:

$$Q_{heater} = I \times V \tag{3}$$

where I and V are the current and the voltage, respectively.

Also, the heat obtained from the nanofluid from the corrugated walls is [34,35]:

$$Q_f = \dot{m}_{nf} C_{p,nf} \left(T_{b_{out}} - T_{b_{in}} \right) \tag{4}$$

where $\dot{m}$, $C_{p,nf}$, $T_{b_{out}}$, and $T_{b_{in}}$ are the mass flow rate of the nanofluid, the specific heat of the nanofluid, and the average bulk temperature at outlet and inlet, respectively.

The heat loss from the test module is:

$$Q_{loss} = \frac{Q_{heater} - Q_f}{Q_{heater}} \times 100 \tag{5}$$

The mean variation between the power supplied by the heaters and the heat received by the flowing nanofluid is of the order of 10%.

The average convective heat transfer coefficient is [35]:

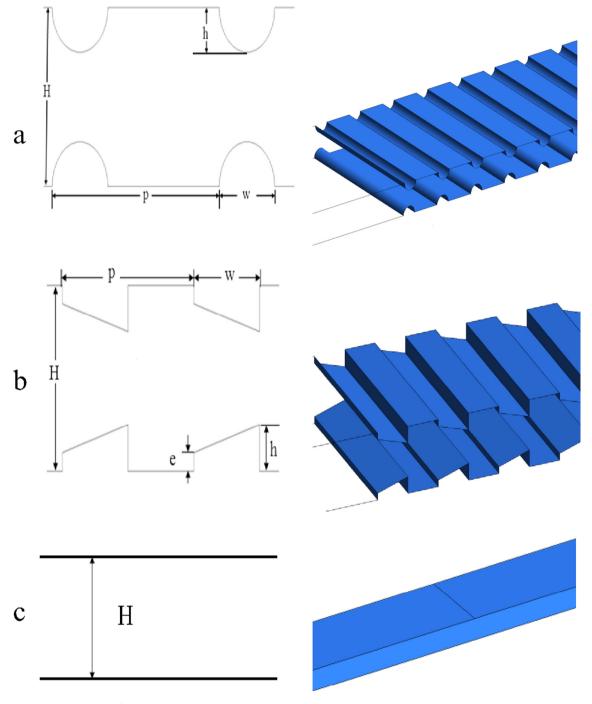$$h_{av} = \frac{Q_f}{A_{conv}(T_{W_{av}} - T_{b_{av}})} \tag{6}$$

Fig. 6. Physical domain of the present study (a) semicircle corrugated channel, (b) trapezoidal corrugated channel, and (c) straight channel.

where A_{conv} is the heated wall area (corrugated walls), and $T_{w_{av}}$ and $T_{w_{av}}$ are average heated wall temperature and average bulk temperature, respectively. $T_{w_{av}}$ and $T_{w_{av}}$ are determined as follows:

$$T_{w_{av}} = \frac{1}{6} \times \sum_{i=1}^{i=6} T_{w_i} \tag{7}$$

$$T_{b_{av}} = \frac{T_{b_{in}} + T_{b_{out}}}{2} \tag{8}$$

Then, the average Nusselt number is [34,35]:

$$Nu_{av} = \frac{h_{av}D_h}{k_{nf}} \tag{9}$$

where k_{nf} is the thermal conductivity of the nanofluid and D_h is the hydraulic diameter of corrugated channel, which can be calculated as follows:

$$D_h = \frac{4A_C}{P} \tag{10}$$

where A_C and P are the cross-sectional area and the wetted perimeter of the flow, respectively.

The friction factor is [35]:

$$f = \Delta p \frac{D_h 2}{L_{corr}\rho_{nf}u_{in}^2} \tag{11}$$

Also, the Reynolds number can be defined as follows [35]:

Fig. 7. Front view of different shapes of test modules (a) semicircle module, (b) trapezoidal module, and (c) straight module.

Table 2
Geometrical structure of corrugated channels.

Parameter	Symbol	Trapezoidal –corrugated channel Value	Semicircle-corrugated channel Value
Channel height	H	10	10
Channel width	W	50	50
Corrugation height	h	2.5	2.5
Corrugation width	w	5	5
Longitudinal pitch	p	15	15
Corrugation- small height	e	1	–

Fig. 8. Boundary conditions of physical model.

$$Re = \frac{\rho u_{in} D_h}{\mu} \qquad (12)$$

where Δp is the differential pressure drop at the test module, L_{corr} is the length of the corrugated channel, ρ_{nf} is the density of nanofluid, and u_{in} is the velocity of nanofluid.

5. Numerical procedure

5.1. Geometrical configuration

The geometry of corrugated channels consists of upper walls, lower walls, and side walls that are straight and unheated. To the corrugated section, the upstream and downstream sections are added to achieve a fully developed flow condition and prevent flow return to the opposite path. These sections are two times and four times longer than the test part (corrugated section), respectively.

In the corrugated section, only upper and lower walls are heated. The width of the channel (W) is five times the height (H) which it is 10 mm. The overall height of the corrugation and the longitudinal pitch are (h) and (p), respectively. Corrugations pitch is equal to 1.5 times channel height.

5.2. Numerical computation and boundary conditions

In this study, the 3-D geometry of the tested channel is completed using SolidWorks premium edition software 2014 × 64 while the heat transfer and flow characteristics of the corrugated models are analyzed using commercial CFD code (FLUENT V.16.1). The finite volume method is chosen to deal with the governing equations, whereas the second-order upwind scheme is applied for convective terms. In this simulation, the k-ε turbulent model is set with enhanced wall treatment functions to resolve the viscous sublayer and improve near–wall treatment. To couple

Table 3
Grid independence test.

Grid number	Average Nusselt number	Relative error%
162,632	126.1311	–
267,696	126.1546	0.018628
329,668	126.1789	0.019258
413,520	126.1896	0.008479
544,235	126.1971	0.005943

Table 4
Accuracy of experimental instruments.

Sensor	Number	Accuracy	Model
Thermocouples	6	±0.1%	Type k-thermocouples
Differential Pressure transducer	1	±0.075%	DPG409-001DWU Omega, USA
Flow meter	1	±5%	Ada-K24F1-1, HaiHuiLai
Temperatures probe	2	±0.16%	EI1034 Temperature Probe, LabJak
Power regulator	1	±0.1	W5SP4vo30-24J
Digital multimeter	1	±1%FS	BK PRECISION, 2831C
Chillier	1	±0.2°C	SPH20N-18-4227
Data logger	1	0.1%	MultiCon SIMEX-CMC-141

velocity and pressure fields, the SIMPLE algorithm is adopted. Moreover, for the diffusion term of the governing equation, the second-order upwind scheme is adopted. The convergence crite-rion is set to 10^{-10} for the energy equation and 10^{-5} for the momentum, continuity, and turbulence equations.

As for model boundary conditions, all walls except the corrugated walls are regarded as adiabatic as shown in Fig. 8. A constant heat flux condition of 10,000 (W/m²), is applied to the corrugated walls, including top and bottom walls of the test section. Velocity inlet is based on Reynolds numbers from 10,000 to 30,000 according to Eq. (12). In this respect, uniform velocity is adopted at the inlet of the tested channel as temperature was kept constant at 300 K. Furthermore, turbulence levels at the inlet are specified as 0.05 and non-slip conditions are applied to all walls.

5.3. Governing equations

Based on the above boundary conditions, 3-D governing equations are established to describe the flow problem and heat transfer as follows:

Continuity equation:

$$\nabla.(\rho_f V) = 0 \tag{13}$$

Momentum equation:

$$\nabla.(\rho_f VV) = -\nabla p + \nabla.\tau \tag{14}$$

Energy equation:

$$\nabla.\left(\rho_f V C_{pf} T\right) = \nabla.(k_f \nabla T - C_{pf} \rho_f \bar{v} t) \tag{15}$$
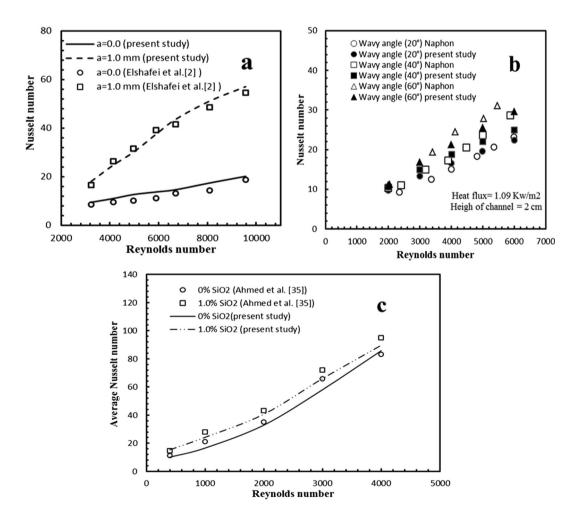

Fig. 9. Comparison between the current work and the outcomes of experimental studies (a) Elshafei et al. [2], and (b) Naphon [8] and with experimental data of (c) Ahmed et al. [35].

The k − ε turbulence model is employed in this study's simulations [37]. Furthermore, mathematical formulas were modified due to the effect of mean velocity gradients in terms of turbulent kinetic energy (G) as shown below [22]:

$$\nabla.(\rho_m V k) = \nabla.\left(\frac{\mu_{t,m}}{\sigma_k}\nabla k\right) + G_m - \rho_m\varepsilon \tag{16}$$

$$\nabla.(\rho_m V \varepsilon) = \nabla.\left(\frac{\mu_{t,m}}{\sigma_\varepsilon}\nabla \varepsilon\right) + \frac{\varepsilon}{k}(C_1 G_m - C_2\rho_m\varepsilon) \tag{17}$$

where

$$\mu_{t,m} = \rho_m C_\mu \frac{K^2}{\varepsilon}, C_1 = 1.44, C_2 = 1.92, C_\mu = 0.09 = 0.09,$$
$$\sigma_k = 1.0, \sigma_\varepsilon = 1.3.$$

5.4. Grid independence test and validation

Using a semicircle-corrugated channel at $Re = 10000$, a grid independence test is established using pure water. The number of mesh elements is been changed in the test from 162,632 elements to 544,235 elements. Accordingly, Eq. (18) displays the relative error between (M1) and (M2), which represents the new outcome and previous outcomes of the Nusselt number, respectively. To compare Nu_{av}, a grid of 413,520 elements is set for simulation as shown in Table 3.

$$e = \left|\frac{M_1 - M_2}{M_1}\right| \times 100 \tag{18}$$

To check the accuracy of the numerical procedure, simulation outcomes are validated with the experimental data obtained from [2] and [8] as presented in Fig. 8a and b, respectively. Accordingly, comparison results show reasonable agreement. For further validation, the nanofluid model in the corrugated channel is compared with the experimental data of Ahmed et al. [35] as presented in Fig. 8c. The outcomes are in good agreement in terms of Nu_{av}.

6. Uncertainties

To reduce experimental error, uncertainty measurements are performed for instruments and other work sources. For this purpose, device calibration was done prior to use. Reynolds and Nusselt numbers are experimental data parameters that are affected by many variables such as flow rate, temperature measurement, and pressure drop. Therefore, Kline and McClintock [38] method is applied for experimental data uncertainty. Due to some independent variables, uncertainties in calculating (W_R^+) were obtained as follows:

$$W_R^+ = \sqrt{\left(\frac{\partial R^+}{\partial X_1}w_1\right)^2 + \left(\frac{\partial R^+}{\partial X_2}w_2\right)^2 + \left(\frac{\partial R^+}{\partial X_3}w_3\right)^2 + \ldots + \left(\frac{\partial R^+}{\partial X_n}w_n\right)^2} \tag{19}$$

where $w_1, w_2, \cdots\cdots w_n$ are the uncertainties of directly measured values. Uncertainty calculations are ±6.66% for Nusselt number, ±5.17% for Reynolds number, and ±10.443% for friction factor, respectively. Table 4 shows the accuracy of the experimental instruments.

7. Results and discussions

Prior to discussing the use of corrugated channels and nanofluids, it is essential to test the validation and accuracy of the experimental system. In this light, the experimental results of the flat channel using water as a working fluid are compared with the

standard correlations of Dittus-Boelter [39] Eq. (20) and Gnielinski [40] Eq. (21) in regard to the Nusselt number, and with Petukhov [41] Eq. (22) for the friction factor.

$$Nu = 0.023Re^{0.8}Pr^{0.4} \tag{20}$$

$$Nu_{av} = \frac{(f/8)(Re - 1000)Pr}{1 + 12.7(f/8)^{0.5}\left(Pr^{2/3} - 1\right)} \tag{21}$$

$$f = (0.79\ln(Re) - 1.64)^{-2} \tag{22}$$

Fig. 9 compares the Nu and friction factor for the current straight channel with standard correlations, which shows good agreement with maximum deviations less than ∓3.2%, ±2%, and ±5.2%, respectively. The outcomes of the straight channel are employed to normalize the corrugated channels results. In this way, the outcomes obtained from the current experimental facility are reliable and dependable.

Fig. 10 shows the velocity and isotherm contours for silica nanofluid flow through channels under consideration at $Re = 10000$ and $\phi = 1\%$. The velocity represented the master key in drag reduction and heat transfer augmentation. In general, corrugations manipulate the fluid path of the main flow, which helps to induce secondary flow vortexes, which enhance heat transfer. In this respect, velocity near the corrugated walls is affected by corrugation shapes and Reynolds number. Furthermore, vortexes occurred between corrugations near the upper and lower corrugated walls where the flow is opposite the prime flow and is more
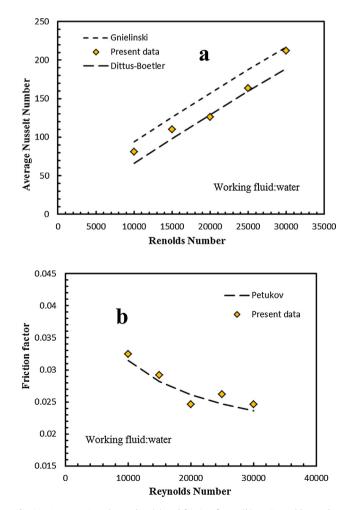

Fig. 10. Average Nusselt number (a) and friction factor (b) vs. Reynolds number.
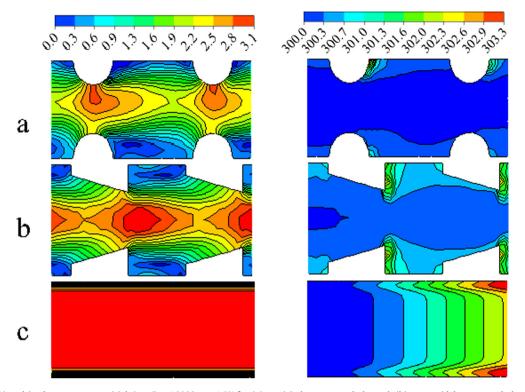
Fig. 11. Velocity (left) and isotherms contours (right) at $Re = 10000$, $\phi = 1.0\%$ for (a) semicircle-corrugated channel, (b) trapezoidal-corrugated channel, and (c) straight channel.
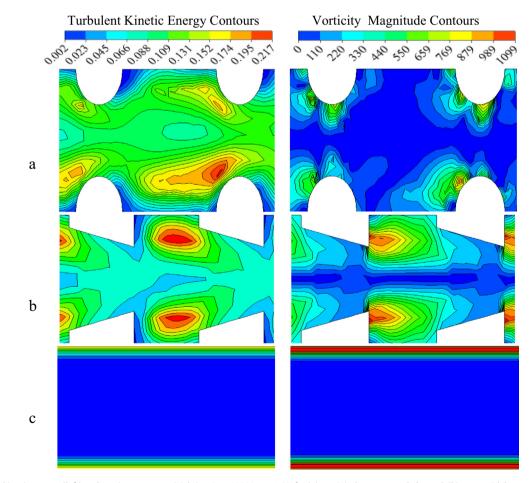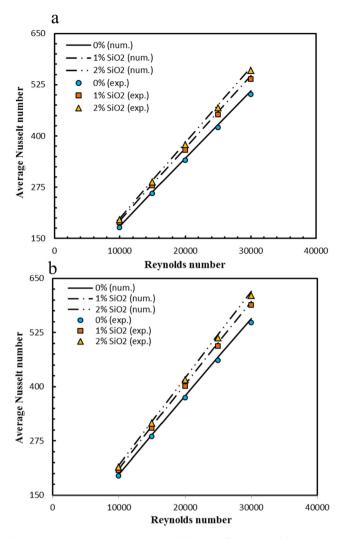

Fig. 12. Turbulent kinetic energy (left) and vortices contours (right) at $Re = 10000$, $\phi = 1.0\%$ for (a) semicircle-corrugated channel, (b) trapezoidal-corrugated channel, and (c) straight channel.

Fig. 13. Average Nusselt number Vs. Reynolds number for (a) Semicircle corrugated channel; (b) Trapezoidal corrugated channel.

Fig. 14. Pressure drop vs. Reynolds number for (a) Semicircle corrugated channel; (b) Trapezoidal corrugated channel.

troubled than in the straight section. As flow increases, secondary flow is expanded the main flow. Additionally, the mixing between the core and the corrugated walls will increase further.

For temperature contours, high-temperature zones are just upstream and downstream of the corrugations for all cases, depending on recirculation flows. Fluid separation occurred between corrugations before and after they caused recirculation in the channel flow (in the opposite path of prime flow). In this respect, the blending between the core (cold) and corrugated walls (hot) is excellent. As a result, temperature gradients increment increase with increasing Reynolds number due to the reduction of thermal boundary layers as well as the induction of a secondary flow in the corrugated part of the walls.

Fig. 11 shows the turbulent kinetic energy and vorticity contours for silica nanofluid flow through the tested shapes at *Re* = 10000 and $\phi = 1\%$. One can conclude from this figure that the intensity of turbulence is significantly affected by corrugation geometrical structures, which increases turbulent heat transfer. With this system, the high turbulent intensity is shown near the corrugation before and after the corrugated channels. In this way, there is a difference between turbulent kinetic energy distribution near the upper and lower walls depending on the form of corrugation. Furthermore, important factors helped generate more turbulent kinetic energy, which are flow type and Reynolds number. Accordingly, high Reynolds number and turbulent flow increase
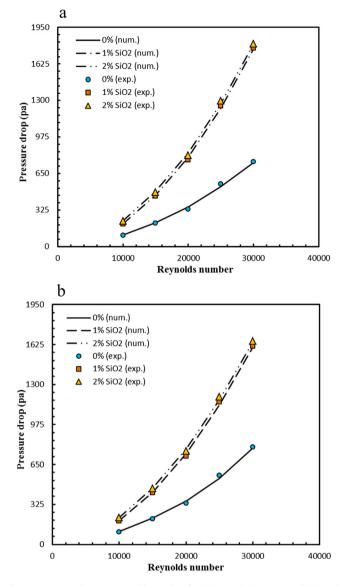
momentum and heat transfer among fluid layers as well as core flow, and wake flow, which creates turbulence opposite the flow. On this basis, the TCC form is best in terms of turbulent energy due to its sharp edges.

For the vorticity contours, vorticity fields are shown to have symmetrical axial directions for all forms. Also, the flow profile of the vorticity contours has an excellent correlation with turbulent kinetic energy. In general, every vorticity generated in the flow path is a pure phenomenon linked to the geometrical structures of the tested channel and flow circumstances. Hence, the generated vortices significantly improved heat exchange due to its positive impact on fluid blending inside the channel. On the other hand, shear stress increases because the working fluid is driven from outside of the boundary layer toward the walls, which generates more friction. Thus, the thermal performance of the tested channel strongly depends on the generation of vortices.

Experimental and numerical results for the Nu_{av} against Re in TCC and SCC at various volume fractions (0, 1.0% and 2.0%) are presented in Fig. 12. Generally, an increase of Reynolds number strongly increases Nu_{av}. In other words, the average Nusselt number for both channels under consideration increased with

increasing Reynolds number due to an increase in the wall temperature gradient. Trouble flow is related to increase in velocity, which improved heat transfer. Furthermore, Nu_{av} increases with increases in volume fraction of nanoparticles due to the boosted thermal conductivity of the water from the addition of SiO_2 particles. The average deviations between numerical and experimental results display good agreement of approximately 9.2% and 8.7% for TCC and SCC, respectively.

Variations of pressure drop (Δp) versus Reynolds number for silica nanofluid at different ϕ for both channels (trapezoidal and semicircle) are shown in Fig. 13. The results show that Δp increases as ϕ increases. This means that an increase of nanoparticles volume fraction increasing nanofluid viscosity and wall shear stress. Furthermore, pressure drop increases as Re increases. The reason behind this is that as volume fraction increased so did velocity. The average deviation values of the numerical outcomes show reasonable agreement with the experimental outcomes. The average deviation is 8.7% and 8.1% for the semicircle and trapezoidal corrugated channel, respectively.

Fig. 14 demonstrates the enhancement ratio of average Nusselt number (ER) in the tested channels to pure water flow in the smooth channel. Nanofluid ER represents the heat transfer performance of the tested cases. ER decreases for all cases with increasing Reynolds number. In addition, there is a low tendency for increases in Re to increase ER for all tested channels. Also, the increase of volume fraction improved heat transfer for the same value of Re. Moreover, it can be unmistakably noted that a volume

fraction of 2.0% is the highest recorded enhancement for both the trapezoidal and semicircle corrugated channel.

Variations in Nu_{av} versus Re for silica nanofluid at $\phi = 2.0\%$ in semicircle, trapezoidal, and straight channels are shown in Fig. 15. Due to increases in Re for every case, Nu_{av} obviously increases extensively and incrementally in both the numerical and experimental results. In other words, there is a marked impact from the corrugation profile on the improvement of the Nu rate. As they have no corrugations, the flat channel flow has the lowest HTC rates among the tested channels. In contrast, channels that have corrugations changed the fluid path of the main flow, which helps induce secondary flow vortexes, which improve heat transfer. Accordingly, TCC offers the highest heat transfer rate while the SC has the lowest values.

The results of pressure drop on the Re of the SiO_2–water nanofluid at $\phi = 2.0\%$ in semicircle, trapezoidal, and straight channels are presented in Fig. 16. In general, the corrugated channels offer a greater pressure drop than flat channel. The extra effects of recirculation zones are the result of corrugations influence, which became more intense depending on the shape of the corrugation.
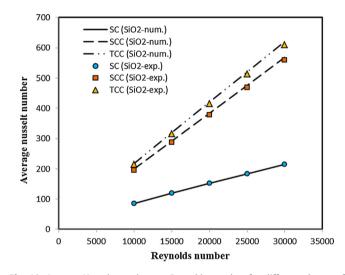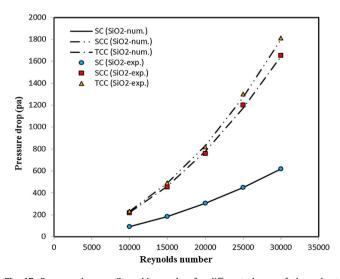

Fig. 16. Average Nusselt number vs. Reynolds number for different shapes of channels at ϕ = 2%.
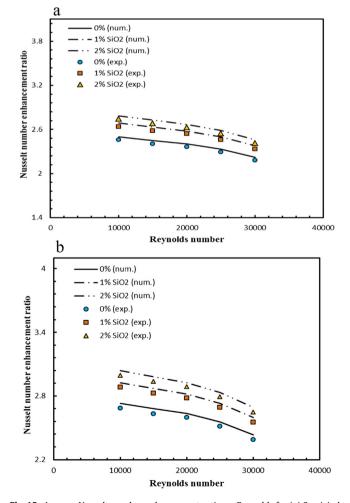

Fig. 15. Average Nusselt number enhancement ratio vs. Reynolds for (a) Semicircle corrugated channel; (b) Trapezoidal corrugated channel.

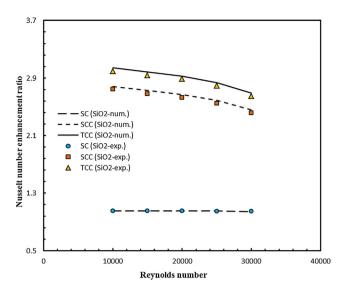Fig. 17. Pressure drop vs. Reynolds number for different shapes of channels at ϕ = 2%.

Fig. 18. Average Nusselt number enhancement ratio vs. Reynolds for different shapes of channels at ϕ = 2%.

As the sharp front edge of the corrugated walls boosted shear stress near the corrugated walls, TCC offers a highest pressure drop than the SCC and SC channels. Therefore, corrugation configuration has a positive influence on heat transfer improvements and a negative impact from increases pressure drop.

Fig. 17 compares the ER for silica nanofluid at $\phi = 2.0\%$ flow in different channels to the flowing of the base fluid (water) in the straight channel. For all channels, ER decreases with increases in Re. In addition, increases in Re increases ER for all tested fluids. SC has the poorest performance over ta range of Re due to its lack of corrugations. Accordingly, TCC has the highest ER, followed by SCC and SC. As a result, with 3.1 at Re = 10000 and ϕ = 2.0%, TCC has the highest enhancement ratio (see Fig. 18).

8. Conclusion

In this study semicircle, trapezoidal, and straight channels are numerically and experimentally tested using SiO_2-water nanofluids. The studies cover ϕ from 0.0 to 0.02 and Re from 10,000 to 30000. The noticeable findings are summarized as follows:

- It is found that corrugations manipulated the fluid path of the main flow, which helped induce secondary flow vortexes that improve heat transfer.
- The use of corrugated channel is advantageous to enhance heat transfer on one hand and on the other hand it introduces undesirable pressure drop in the system. Much better performance in terms of heat transfer is observed with SiO_2-water nanofluid over the conventional base fluid.
- Both average Nusselt number and pressure drop increase with increasing Reynolds number for all channel shapes. However, the impact of Reynolds number on average Nusselt number and pressure drop for TCC is higher than SCC and SC.
- For all tested channels, one observable point is that Nusselt number, pressure drop, and enhancement ratio increase as the volume fraction of SiO_2 increases. For instance, at the same Reynolds number, ER increases from 2.82 to 3.1 when ϕ increases from 1% to 2%.
- The enhancement ratio (ER) displays decreases with increasing Reynolds number and increases with increasing volume fractions.

- The enhancement ratio of the TCC is superior to SCC and SC. It is found that the maximum ER of TCC is 3.1 at Re = 10000 and ϕ = 2.0%.
- Finally, a new style of TCC is experimentally and numerically recommended as the best choice to obtain thermal improvement in heat exchange devices.

Declaration of Competing Interest

None.

References

[1] N. Piroozfam, A.H. Shafaghi, S.E. Razavi, Numerical investigation of three methods for improving heat transfer in counter-flow heat exchangers, Int. J. Therm. Sci. 1 (133) (2018) 230–239.
[2] E.A. Elshafei, M.M. Awad, E. El-Negiry, A.G. Ali, Heat transfer and pressure drop in corrugated channels, Energy 35 (1) (2010) 101–110.
[3] M. Akbarzadeh, S. Rashidi, J.A. Esfahani, Influences of corrugation profiles on entropy generation, heat transfer, pressure drop, and performance in a wavy channel, Appl. Therm. Eng. 1 (116) (2017) 278–291.
[4] E. Bayrak, A.B. Olcay, M.F. Serincan, Numerical investigation of the effects of geometric structure of microchannel heat sink on flow characteristics and heat transfer performance, Int. J. Therm. Sci. (2018).
[5] L. Zhang, D. Che, Influence of corrugation profile on the thermalhydraulic performance of cross-corrugated plates, Numer. Heat Transf., Part A: Appl. 59 (4) (2011) 267–296.
[6] H. Pehlivan, Experimental investigation of convection heat transfer in converging–diverging wall channels, Int. J. Heat Mass Transf. 1 (66) (2013) 128–138.
[7] M. Khoshvaght-Aliabadi, F. Nozan, Water cooled corrugated minichannel heat sink for electronic devices: effect of corrugation shape, Int. Commun. Heat Mass Transfer 1 (76) (2016) 188–196.
[8] P. Naphon, Heat transfer characteristics and pressure drop in channel with V corrugated upper and lower plates, Energy Convers. Manage. 48 (5) (2007 May 1) 1516–1524.
[9] N. Zheng, P. Liu, F. Shan, Z. Liu, W. Liu, Numerical investigations of the thermal-hydraulic performance in a rib-grooved heat exchanger tube based on entropy generation analysis, Appl. Therm. Eng. 25 (99) (2016) 1071–1085.
[10] M.H. Fard, M.N. Esfahany, M.R. Talaie, Numerical study of convective heat transfer of nanofluids in a circular tube two-phase model versus single-phase model, Int. Commun. Heat Mass Transf. 37 (1) (2010) 91–97.
[11] M.K. Abdolbaqi, C.S. Azwadi, R. Mamat, W.H. Azmi, G. Najafi, Nanofluids heat transfer enhancement through straight channel under turbulent flow, Int. J. Autom. Mech. Eng. 1 (11) (2015) 2294.
[12] M. Rostamani, S.F. Hosseinizadeh, M. Gorji, J.M. Khodadadi, Numerical study of turbulent forced convection flow of nanofluids in a long horizontal duct considering variable properties, Int. Commun. Heat Mass Transf. 37 (10) (2010 Dec 1) 1426–1431.
[13] A.R. Sajadi, M.H. Kazemi, Investigation of turbulent convective heat transfer and pressure drop of TiO2/water nanofluid in circular tube, Int. Commun. Heat Mass Transfer 38 (10) (2011) 1474–1478.
[14] S.Z. Heris, M.N. Esfahany, S.G. Etemad, Experimental investigation of convective heat transfer of Al2O3/water nanofluid in circular tube, Int. J. Heat Fluid Flow 28 (2) (2007) 203–210.
[15] M. Esmaeili, K. Sadeghy, M. Moghaddami, Heat transfer enhancement of wavy channels using Al2O3 nanoparticles, J Enhanc Heat Transf 17 (2) (2010) 139.
[16] R.K. Ajeel, W.S. Salim, K. Hasnan, Impacts of corrugation profiles on the flow and heat transfer characteristics in trapezoidal corrugated channel using nanofluids, J. Adv. Res. Fluid Mech. Therm. Sci. 49 (2) (2018) 170–179.
[17] R.K. Ajeel, W.I. Salim, K. Hasnan, Thermal and hydraulic characteristics of turbulent nanofluids flow in trapezoidal-corrugated channel: Symmetry and zigzag shaped, Case Stud. Therm. Eng. 1 (12) (2018) 620–635.
[18] R.K. Ajeel, W.I. Salim, K. Hasnan, Thermal performances comparison in various types of trapezoidal corrugated channel using nanofluids, Int. Rev. Mech. Eng. 12 (8) (2018) 672–683.

[19] R.K. Ajeel, W.S. Salim, K. Hasnan, Numerical investigations of flow and heat transfer enhancement in a semicircle zigzag corrugated channel using nanofluids, Int. J. Heat Technol. 36 (4) (2018) 1292–1303.

[20] R.K. Ajeel, W.I. Salim, K. Hasnan, Comparative study of the thermal performance of corrugated channels using ZnO–water nanofluid, J. Thermophys. Heat Transf. 1–9 (2018).

[21] R.K. Ajeel, W.I. Salim, K. Hasnan, Thermal performance comparison of various corrugated channels using nanofluid: numerical study, Alexandr. Eng. J. (2018).

[22] R.K. Ajeel, W.I. Salim, K. Hasnan, Design characteristics of symmetrical semicircle-corrugated channel on heat transfer enhancement with nanofluid, Int. J. Mech. Sci. 1 (151) (2019) 236–250.

[23] R.K. Ajeel, W.S. Salim, K. Hasnan, Heat transfer enhancement in semicircle corrugated channel: effect of geometrical parameters and nanofluid, J. Adv. Res. Fluid Mech. Therm. Sci. 53 (1) (2019) 82–94.

[24] R.K. Ajeel, W.I. Salim, K. Hasnan, Influences of geometrical parameters on the heat transfer characteristics through symmetry trapezoidal-corrugated channel using SiO2-water nanofluid, Int. Commun. Heat Mass Transf. 1 (101) (2019) 1–9.

[25] P. Naphon, S. Wiriyasart, Pulsating flow and magnetic field effects on the convective heat transfer of TiO2-water nanofluids in helically corrugated tube, Int. J. Heat Mass Transf. 31 (125) (2018) 1054–1060.

[26] S. Pavlovic, E. Bellos, R. Loni, Exergetic investigation of a solar dish collector with smooth and corrugated spiral absorber operating with various nanofluids, J. Clean. Prod. 10 (174) (2018) 1147–1160.

[27] M. Khoshvaght-Aliabadi, A. Zamzamian, F. Hormozi, Wavy channel and different nanofluids effects on performance of plate-fin heat exchangers, J. Thermophys. Heat Transf. 28 (3) (2014) 474–484.

[28] A.A. Alfaryjat, H.A. Mohammed, N.M. Adam, D. Stanciu, A. Dobrovicescu, Numerical investigation of heat transfer enhancement using various nanofluids in hexagonal microchannel heat sink, Therm. Sci. Eng. Prog. 1 (5) (2018) 252–262.

[29] S.M. Fotukian, M.N. Esfahany, Experimental investigation of turbulent convective heat transfer of dilute γ-Al2O3/water nanofluid inside a circular tube, Int. J. Heat Fluid Flow 31 (4) (2010) 606–612.

[30] A. Raisi, B. Ghasemi, S.M. Aminossadati, A numerical study on the forced convection of laminar nanofluid in a microchannel with both slip and no-slip conditions, Numer. Heat Transf., Part A: Appl. 59 (2) (2011) 114–129.

[31] M. Khoshvaght-Aliabadi, M. Tatari, M. Salami, Analysis on Al2O3/water nanofluid flow in a channel by inserting corrugated/perforated fins for solar heating heat exchangers, Renew. Energy 1 (115) (2018) 1099–1108.

[32] O. Manca, S. Nardini, D. Ricci, A numerical study of nanofluid forced convection in ribbed channels, Appl. Therm. Eng. 1 (37) (2012) 280–292.

[33] M.A. Ahmed, N.H. Shuaib, M.Z. Yusoff, A.H. Al-Falahi, Numerical investigations of flow and heat transfer enhancement in a corrugated channel using nanofluid, Int. Commun. Heat Mass Transf. 38 (10) (2011) 1368–1375.

[34] W. Arshad, H.M. Ali, Experimental investigation of heat transfer and pressure drop in a straight minichannel heat sink using TiO2 nanofluid, Int. J. Heat Mass Transf. 1 (110) (2017) 248–256.

[35] M.A. Ahmed, M.Z. Yusoff, K.C. Ng, N.H. Shuaib, Numerical and experimental investigations on the heat transfer enhancement in corrugated channels using SiO2–water nanofluid, Case Stud. Therm. Eng. 1 (6) (2015) 77–92.

[36] A.H. Al-Waeli, M.T. Chaichan, H.A. Kazem, K. Sopian, Comparative study to use nano-(Al2O3, CuO, and SiC) with water to enhance photovoltaic thermal PV/T collectors, Energy Convers. Manage. 15 (148) (2017 Sep) 963–973.

[37] B.E. Launder, D.B. Spalding, Mathematical Models of Turbulence, Academic press, 1972.

[38] F. McClintock, Describing uncertainties in single-sample experiments, Mech. Eng. 75 (1) (1953) 3–8.

[39] F.P. Incropera, P.D. DeWitt, T.L. Bergman, A.S. Lavine, Fundamentals of Heat and Mass Transfer, John-Wiley & Sons, 2006.

[40] V. Gnielinski, New equations for heat and mass transfer in turbulent pipe and channels flow, Int. Chem. Eng. 16 (1976) 359–368.

[41] B.S. Petukhov, V.N. Popov, Theoretical calculation of heat exchange in turbulent flow in tubes of an incompressible fluid with variable physical properties, High Temperature 1/1 (1963) 69–83. see also B.S. Petukhov, V.V. Kirillov, The problem of heat exchange in the turbulent flow of liquids in tubes, (in Russian) Teploenergetika 4/4 (1958) 63–68.